Crystal Plasticity Based Finite Element Modeling in Polycrystalline Ti-7Al Alloys

by

Chengcheng Tao

A thesis submitted to The Johns Hopkins University in conformity with the requirements for the degree of Master of Science.

Baltimore, Maryland

August, 2014

Abstract

This thesis develops an experimentally calibrated computational model based on crystal plasticity for the analysis of α-Ti-7Al polycrystalline alloys. The crystal plasticity finite element model uses rate and size-dependent anisotropic elasto plasticity constitutive law. The study contains a combination of orientation imaging microscopy (OIM), misorientation, microtesting, computational simulations and minimization process, including genetic algorithms for calibration of the material parameters and characterization. Size effects are also taken into consideration in the analysis. The polycrystalline Ti-7Al computational model involves statistically equivalent orientation distributions to those observed in the orientation imaging scans. Simulations detected effects of orientation, misorientation and microtexture distributions through simulations. Constant strain rate test is simulated with this model, and the results are compared with experiments.

Primary Reader: Professor Somnath Ghosh

Secondary Reader: Professor Jaafar El-Awady

Acknowledgements

I would like to acknowledge and thank my advisor, Dr. Somnath Ghosh, for his encouragement, support, constructive advice, and valuable technical training during the past 2 years. His guidance, insight, and drive were the single largest factor in the completion of the thesis. I also appreciate Professor El-Awady's careful review and detailed comments for my work.

I must also thank all my colleagues at Computational Mechanics Research Laboratory, who I continually relied upon for assistance. I would like to particularly thank Jiahao Cheng, Ahmad Shahba for their time and efforts in personally helping me with my project during these entire 2 years. I owe a lot of my training in computational mechanics to their willingness to help and mentor me even through times where they had their own work to do.

Special thanks to Dr. Adam Pilchak from Air Force Research Laboratory for his adequate experiment data as well as patient collaboration with us during the project.

I also acknowledge the financial support of Army Research Laboratory and computer support by the Homewood High Performance Compute Cluster.

Contents

List of Tables

List of Figures

Chapter 1

Introduction

Titanium alloys are widely used in a number of applications from aerospace, medical, sporting goods industries [1] because of their high strength (~700-1000Mpa), low density, high fracture toughness and corrosion resistance [2]. These alloys exhibit a cold creep phenomenon. Time dependent deformation is seen to happen at room temperature and at loads as 60% of yield strength [3-7]. The cold creep mechanism occurs due to dislocation glide where dislocations are arrayed in a planar fashion instead of diffusion-mediated at low homologous temperatures. It is mainly dependent on crystallographic orientation features directly affect mechanical properties of polycrystalline materials.

Transmission electron microscopy study has shown that deformation is caused by dislocation glide, where the dislocations are inhomogeneously distributed into planar arrays. The planarity of slip has been attributed to the effect of short range ordering of Ti and Al atoms on the HCP lattice [8]. In addition, creep strains can accumulate at applied stresses significantly smaller than the yield strength. In this way, titanium alloys are chosen

widely in high performance structural applications where dimensional tolerance is a critical factor.

Ti alloy shows rate sensitivity values typically that are similar from those observed in other metallic alloys that do not display a similar low temperature creep behavior [9]. It has also been recognized that crack initiation in Ti is related with grains that have the [0 0 0 1] crystal orientations close to the deformation axis. A number of references have been speculated for this effect [10], which shows that local load shedding between grains of different orientations has a significant effect on this behavior.

In pure Ti and its alloys, plastic deformation depended on the crystal orientation considerably. These HCP materials exhibit complex modes of deformation due to their low symmetries. The inelastic deformation is highly anisotropic because of the difference in deformation resistances in different slip systems of the crystals [11]. For example, single crystals α-Ti-6Al are significantly stronger when the deformation axis is parallel to the [0 0 0 1] direction of the crystal [10]. In this orientation, $<c+a>$ dislocation slip on pyramidal planes is activated. In this situation, critical resolved shear strength (CRSS) is much larger than the CRSS for $<a>$ dislocation slip on basal or prismatic planes. And the planar slip causes the strain hardening exponents of Ti alloys quite small [8]. This makes the effect of grain

boundaries and interfaces on deformation important. With little intrinsic ability to strain hardening, planar slip bands propagate across favorably oriented grains upon initial loading. Large local stress concentrations consequently develop in neighboring grains, which are less favorably oriented for <*a*>-type slip. Local stresses are particularly large when favorably oriented with its <*c*>-axis parallel to the macroscopic deformation direction [12].

The disadvantage in experiments is the large cost for processing and testing real samples as well as varying one microstructural feature while holding the other constant because of their highly coupled characteristics [13]. Image-based modeling and simulation with crystal plasticity finite element method analyses of polycrystalline microstructures is a good option compared to experimental methods for determining microstructure-property relationships. The models by Groeber [14] represent the characteristics of crystallographic orientations, misorientations, grain morphology and distributions for good predictive capability. Compared with experiment, it's easy to vary the microstructural features of these specimens independently to get a direct understanding of the effect on properties. It's important that the models be experimentally validated and efficient for simulating a large number of grains in the polycrystalline aggregate [15-16].

Rate dependent and independent crystal plasticity models have been developed in literature to predict anisotropy due to crystallographic texture evolution, e.g. in [17-19]. Anand *et al.* have developed experiment based crystal plasticity computational models for OHFC copper (fcc) [20], aluminum (fcc) [11] and tantalum (bcc) [21]. Curve fitting to polycrystalline experimental data is used to obtain material parameters. By comparing its predictions for stress-strain relation and texture evolution, the predictive capability of the model is evaluated. Robust computational and experimental effort for titanium (hcp) at high temperatures has also been reported by Balasubramanian and Anand [11, 22]. Slip system data for crystal plasticity parameters have been calibrated from single crystal experiments with polysyntetically twinned α_2-Ti_3Al and Ti-6Al by Grujicic, Batchu and Hasija [23]. Kad [24] have used these single crystal based parameters to model polycrystalline material behavior.

The present thesis aims to develop a quantitative understanding of the role of microstructure on the rate-dependent plastic response of the titanium alloy Ti-7Al using a comprehensive CPFEM analysis based approach. The overall process encompasses 2D microstructural characterization, 3D microstructure model creation, mesh generation and subsequently, CPFEM analysis and data processing. Quantitative characterization of material

microstructures is accomplished through SEM image analysis, EBSD data collection, stereological procedures and statistical quantification. Subsequent to material characterization and data acquisition, a 3D reconstruction code developed in [14-16] is used to create statically equivalent, virtual microstructures that are meshed for computational simulations. Crystal plasticity finite element method simulations and analyses are conducted for strain-rate controlled and compared with experimental results for calibrating the model. In order to gain an understanding of sensitivities to the microstructure, virtual microstructures with varying characteristic functions are generated and analyzed.

Chapter 2

Material description and model

2.1 Material description

The material studied in this work is single-phase α-Ti-7Al which has an HCP crystal structure. Close-packed layers of atoms are stacked in the order ABABAB so that the hexagonal crystal structure is created. Every third layer is in exactly the same relative position as the first. The interatomic spacing on the A plane is denoted by *a* while the spacing between adjacent A planes is denoted by *c*. The ratio *c/a* is termed the axial ratio, which is different in different hexagonal materials. Titanium has an axial ratio of *c/a*=1.587.

The material basis vectors corresponding to the HCP lattice structure are denoted by a set of nonorthogonal base vectors, $\{\mathbf{a_1}, \mathbf{a_2}, \mathbf{a_3}, \mathbf{c}\}$, with $\mathbf{a_1} + \mathbf{a_2} + \mathbf{a_3} = 0$, as shown Fig.1. For computational simplicity, an orthonormal basis $\{\mathbf{e}_1^c, \mathbf{e}_2^c, \mathbf{e}_3^c\}$ can be derived from these crystallographic vectors [11]. The HCP crystals are made of five different families of slip systems, which are the basal <*a*>, prismatic <*a*>, pyramidal <*a*>, first order pyramidal <*c*+*a*> and second order pyramidal <*c*+*a*> slip systems with a total of 30 slip

system, as shown in Fig 2.1. For elasticity, a transversely isotropic response with five independent elastic constants is used to model the anisotropy [11].

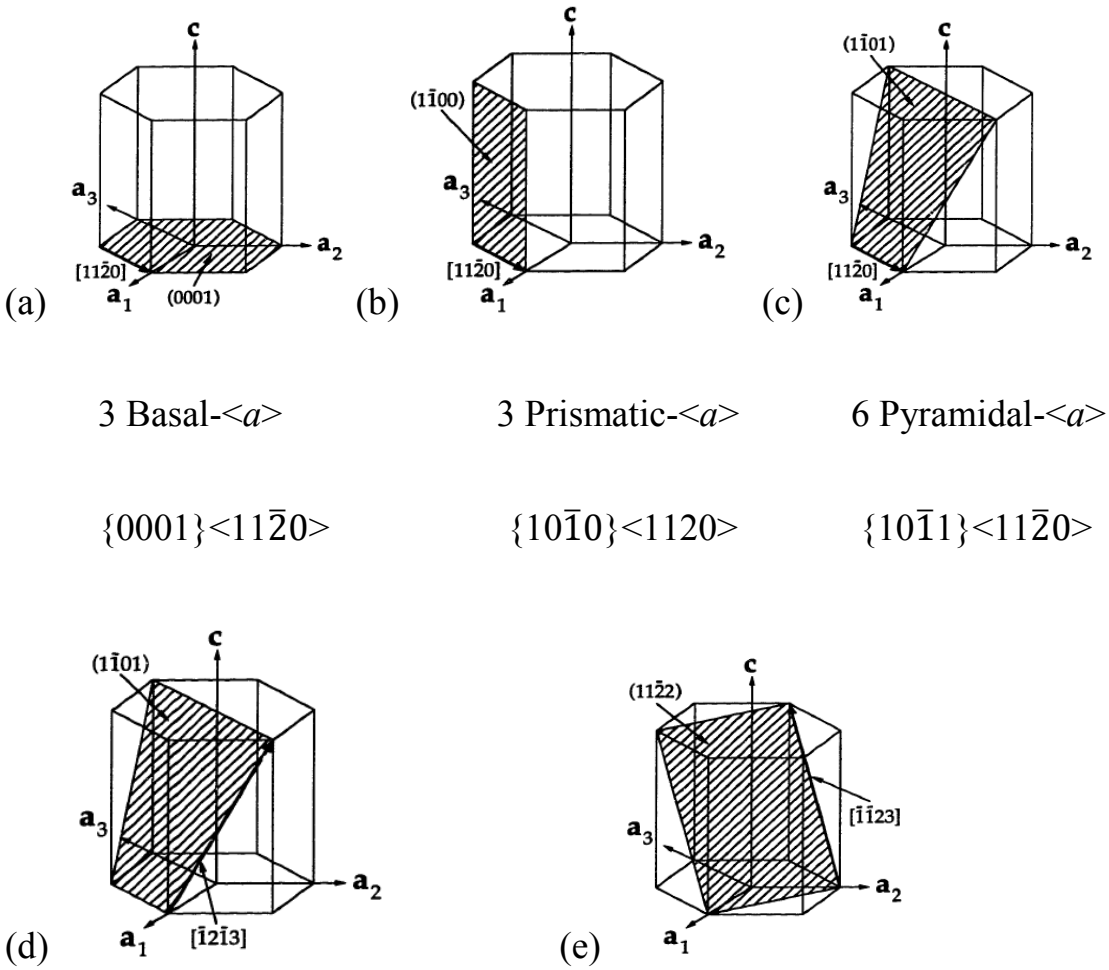

Fig. 2.1 HCP crystal structure and slip systems with non-orthogonal basis. Figure is taken form Balasubramanian [11]

2.2 Crystal plasticity constitutive model

2.2.1 Crystal plasticity based material model

The deformation behavior of Ti-7Al is modeled using a rate-dependent, finite strain, crystal plasticity formulation, which is isothermal, elastic-viscoplastic. In this model, crystal deformation is caused by the elastic stretching and rotation of the crystal lattice and plastic slip on the different slip system.

The stress-strain relation in this model is written in terms of the second Piola-Kirchoff stress ($\mathbf{S}=\det\mathbf{F}^{e}\mathbf{F}^{e-1}\boldsymbol{\sigma}\mathbf{F}^{e-T}$) and the work conjugate Lagrange Green strain tensor ($\mathbf{E}^{e} \equiv (1/2)\{\mathbf{F}^{eT}\mathbf{F}^{e} - \mathbf{I}\}$) as

$$\mathbf{S}=\boldsymbol{C}:\boldsymbol{E}^{e} \tag{1}$$

where $\boldsymbol{C}$ is a fourth order anisotropic elasticity tensor, $\boldsymbol{\sigma}$ is the Cauchy stress tensor and $\mathbf{F}^{e}$ is an elastic deformation gradient defined by the relation

$$\mathbf{F}^{e} \equiv \mathbf{F}\mathbf{F}^{p-1},\ \det\mathbf{F}^{e} > 0 \tag{2}$$

$\mathbf{F}$ and $\mathbf{F}^{p}$ are the deformation gradient and its plastic component, respectively, with the incompressibility constraint $\det\mathbf{F}^{p}=1$. The flow rule governing evolution of plastic deformation is expressed as in terms of the plastic velocity gradient

$$\mathbf{L}^{p} = \dot{\mathbf{F}}^{p}\mathbf{F}^{p-1} = \sum_{\alpha}\dot{\gamma}^{\alpha}\mathbf{s}_{0}^{\alpha} \tag{3}$$

where the Schmidt tensor is expressed as $\mathbf{s}_0^\alpha \equiv \mathbf{m}_0^\alpha \otimes \mathbf{n}_0^\alpha$ in terms of the slip direction ($\mathbf{m}_0^\alpha$) and slip plane normal ($\mathbf{n}_0^\alpha$) in the reference configuration, associated with the αth slip system. The plastic shearing rate $\dot{\gamma}^\alpha$ on the αth slip system is given by the power law relation:

$$\dot{\gamma}^\alpha = \dot{\tilde{\gamma}} \left|\frac{\tau^\alpha}{g^\alpha}\right|^{1/m} sign(\tau^\alpha),\ \tau^\alpha \equiv (\mathbf{C}^e : \mathbf{S}) \cdot \mathbf{s}_0^\alpha \tag{4}$$

$\dot{\tilde{\gamma}}$ is the reference plastic shearing rate, τ^α and g^α are the αth slip system resolved shear stress and the slip system deformation resistance. *m* is the material rate sensitivity parameter and $\mathbf{C}^e$ is the elastic stretch. The slip system resistance is taken to evolve as:

$$\dot{g}^\alpha = \sum_{\beta=1}^{nslip} h^{\alpha\beta} \left|\dot{\gamma}^\beta\right| = \sum_\beta q^{\alpha\beta} h^\beta \tag{5}$$

where $h^{\alpha\beta}$ is the strain hardening rate due to self and latent hardening, h^β is self-hardening rate and $q^{\alpha\beta}$ is a matrix describing the latent hardening. The evolution of the self-hardening rate is governed by the relation:

$$h^\beta = h_0^\beta \left|1 - \frac{g^\beta}{g_s^\beta}\right| \text{sign}(1 - \frac{g^\beta}{g_s^\beta}),\quad g_s^\beta = \tilde{g}(\frac{\dot{\gamma}^\beta}{\dot{\tilde{\gamma}}})^n \tag{6}$$

where h_0 is the initial hardening rate, g_s^β is the saturation slip deformation resistance, and *r*, $\breve{g}$ and *n* are the slip system hardening parameters.

2.2.2 Size dependence in the crystal plasticity model for Ti-7Al

In continuum plasticity, the dependence of the flow stress on the grain size has been expressed by the Hall-Petch relationship in [13, 25]. In crystal plasticity formulation, a similar equation that relates the slip system deformation resistance g^{α} to a characteristic size can be expressed as

$$g^{\alpha} = g_0^{\alpha} + \frac{K^{\alpha}}{\sqrt{D^{\alpha}}} \tag{7}$$

where g_0^{α} and K^{α} are size-effect-related slip system constants that refer to the interior slip system deformation resistance and slope, respectively, and D^{α} is the characteristic length scale governing the size effect. The characteristic length scale (D^{α}) for a single-phase alloy is represented by the average grain size. The crystal plasticity parameters, calibrated for single crystal α Ti-6Al [12], are used in the present for the primary α phase.

Experiments on single crystal α-Ti-7Al have been used in Hasija [12] (2003) to calibrate crystal plasticity parameters for individual slip systems in each of the constituent phases by a genetic algorithm [12, 26, 27] based optimization scheme. The calibrated values of the initial slip system

deformation resistance g^{α} reflect the anisotropy caused by the basal, prismatic and pyramidal slip systems.

Chapter 3

Calibration for material parameters from single crystal experiment data

3.1 Mechanical testing of single α colonies in Ti-7Al microstructure

The computational models in this thesis are calibrated and validated using results of mechanical tests, conducted with samples of single-phase α-Ti-7Al. The single crystal experimental results are provided by Adam Pilchak from Air Force Research Labs. Tension tests are conducted with single crystals, in which samples are each oriented to maximize the resolved shear stress on one of the three <*a*>-type slip directions on the prismatic and basal planes. In addition, tests are conducted with samples for which the [0 0 0 1] axis coincides with the tensile direction.

All single α colonies of Ti-7Al samples for mechanical testing are extracted from successfully grown colonies ranging in size from 5 to 25 mm. Laue back-reflection X-ray techniques are used to identify the crystallographic orientation of the α phase. Scanning electron microscopy (SEM) observations are used to determine the relative alignment of the broad face of the α interface, allowing for the unambiguous identification of the three *a*-type $\{1120\}$ slip directions. A plunge electrical discharge machining process is used to extract dogbone-shaped microtensile samples from the thin oriented single-crystal sections. Microtensile testing of these

samples is performed in a piezo-driven microsample testing machine. Nine tests are conducted at constant strain rates of 1.7×10^{-4}, 5.2×10^{-4}, $9.7\times 10^{-4}\ s^{-1}$ with maximum slip activity on the basal, prismatic, and <c+a> pyramidal slip systems. The experimental results are shown as Fig 3.1.

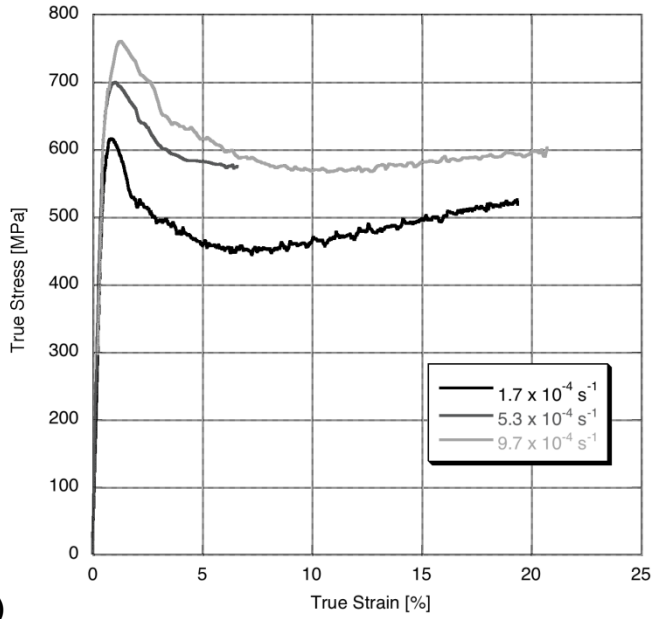

(a)

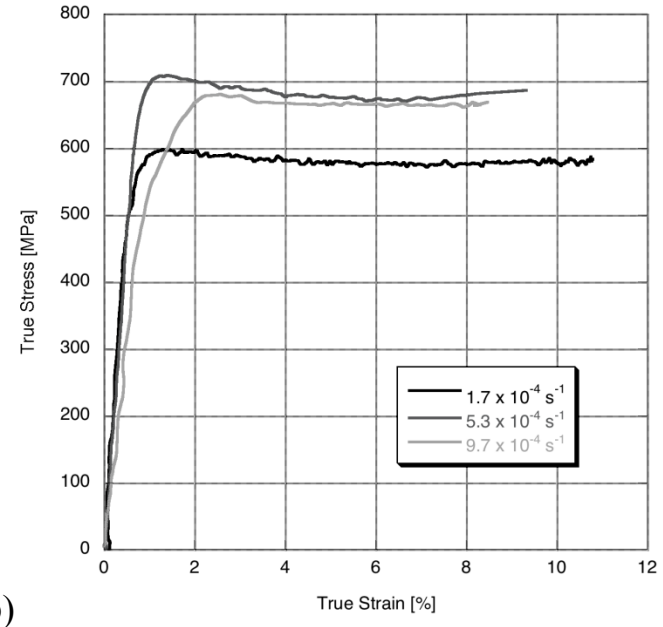

(b)

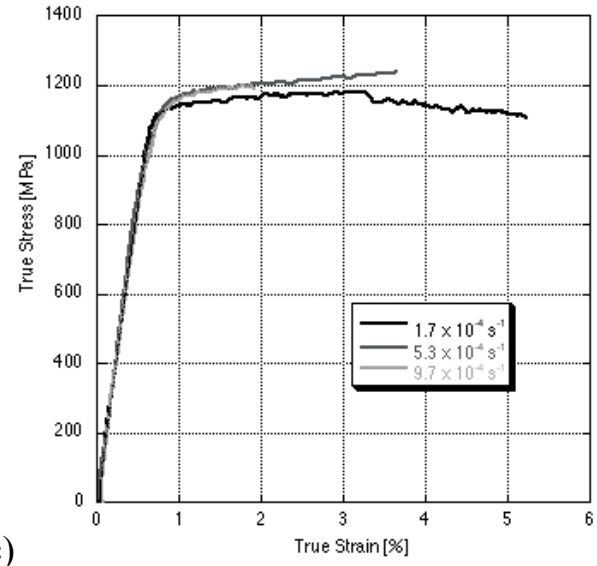

(c)

Fig.3.1 Single crystal Experimental results for different slip systems and constant strain rates. (a) <*a*> basal slip system, (b) <*a*>prismatic slip system, <*c*+*a*> pyramidal slip system.

3.2 Calibration process

The calibration for single crystal includes anisotropic elastic constants and crystal plasticity parameters in each crystal. For calibration purpose, constants strain rate uniaxial tensile tests at rate of $10^{-4}\ s^{-1}$ are conducted with single crystal α-Ti-7Al alloys. Three experiments are set up for maximum slip system activity (maximum Schmid factor) along the basal <*a*>, prismatic <*a*> and pyramidal <*c*+*a*> slip system, respectively. 1296 four-noded tetrahedron elements are used in the single crystal calibration.

The elastic-plastic constitutive relation for finite deformation is incorporated with the UMAT user interface. Displacement boundary condition is applied on the top surface and nodes on the bottom are fixed.

The elastic constants are calibrated by comparing the slope of the experimental stress-strain curve in the constant strain rate test for single crystals with that obtained from the finite element simulations. The material coordinate system is defined by orthonormal basis$\{\mathbf{e}_1^c, \mathbf{e}_2^c, \mathbf{e}_3^c\}$, where the 1, 2, 3 directions are aligned with the [$\bar{1}$ 2 $\bar{1}$ 0], [$\bar{1}$ 0 1 0] and [0 0 0 1] directions of the HCP crystal lattice, respectively. In this system, the components of the elastic stiffness tensor $C_{\alpha\beta}$(α=1,…,6, β=1,…,6) for a transversely isotropic material are determined from the experiment observations to be: C_{11}=C_{22}=165.49 Gpa, C_{12}=114.23 Gpa, C_{13}=C_{23}=66.303 Gpa, C_{33}=208.23 Gpa, C_{44}=25.63 Gpa, C_{55}= C_{66}=65.828 Gpa and all other $C_{\alpha\beta}$'s=0.

Due to the number of parameters required to describe the slip system flow rule, shear resistance relation and the nonlinearity of these equations, genetic algorithm [12, 26, 27] is used in the process of optimization. Of the various parameters calibrated using the experimental results are (i) material rate sensitivity *m*, (ii) the reference plastic shearing rate $\dot{\tilde{\gamma}}$, (iii) the initial

slip system deformation resistance g_0^α, (iv) the initial hardening rate h_0 and (v) various shear resistance evolution related parameters *r*, $\tilde{g}$ and *n*.

Material parameter calibration is conducted in two stages. In the first step, a sensitivity analysis is conducted to determine which parameters affect the response significantly. The key response variables are considered to be the proportional limit (σ_p), initial macroscopic yield strength (σ_y), and the post yield slope (*H*) in the stress-strain curve. For σ_p and σ_y, higher sensitivity is observed with respect to *m*, $\dot{\bar{\gamma}}$, g_0^α. And for *H*, high sensitivity is observed with respect to $\dot{\bar{\gamma}}$, g_0^α, h_0, $\tilde{g}$. High sensitivity is associated with a higher order representation in the minimization.

The second step is the minimization of a suitably chosen objective function with respect to the design variables to obtain parameters for the crystal plasticity constitutive equations for the different hcp slip systems.

3.3 Calibration results

The corresponding calibrated parameters for the three different slip systems are shown in Table 3.1.

Table 3.1 Calibrated parameters for basal <a>, prismatic <a>, pyramidal<a> and pyramidal <c+a>slip systems

Parameters	Basal <a> slip system	Prismatic <a> slip system	Pyramidal <a> slip system	Pyramidal <c+a>slip system
m	0.15	0.15	0.15	0.02
g_0(MPa)	327	326	500	1000
$\dot{\bar{\gamma}}(s^{-1})$	0.005	0.002	0.002	0.006
h_0	500	300	500	600

r	0.5	0.5	0.5	0.1
n	0.1	0.1	0.1	0.01
$\tilde{g}$(MPa)	500	600	750	1650

In order to simulate the yield point phenomenon in basal and prismatic experiment result, an expression for $\dot{\tilde{\gamma}}$ for HSLA steel [26] is added as a function of plastic strain:

$$\dot{\tilde{\gamma}} = \dot{\gamma}_0 \left\{ \frac{\tanh\left[K^*\left(\overline{\varepsilon^p} - l_p\right)\right] + tanh\left(Kl_p\right)}{\tanh(K) + \tanh(Kl_p)} \right\} \tag{8}$$

where $\overline{\varepsilon^p}$ is the equivalent plastic strain defined as $\overline{\varepsilon^p} = \sqrt{\frac{2}{3}\varepsilon_{ij}^p \varepsilon_{ij}^p}$, and the Lagrangian plastic strain is defined as $\varepsilon_{ij}^p = \frac{1}{2}(F_{ij}^{pT} F_{ij}^p - \delta_{ij})$. Equation (8) assumes that $\dot{\tilde{\gamma}}$ is the same for all slip systems initially. It increases rapidly with plastic strain. K and l_p are material constants in this equation.

Table 3.2 Calibrated parameters for yield point phenomenon in each slip system

Slip system	$\dot{\gamma}_0$	K^*	l_p	K

Basal <a> slip system	0.005	32	0.038	10^4
Prismatic <a> slip system	0.002	3	0.02	23
Pyramidal <a> slip system	0.002	32	0.01	10^4
Pyramidal <c+a>slip system	0.006	0	0.01	10^4

Stress strain plots, comparing the experimental and computational results with the calibrated parameters, are shown for the three slip systems in Fig 3.1.

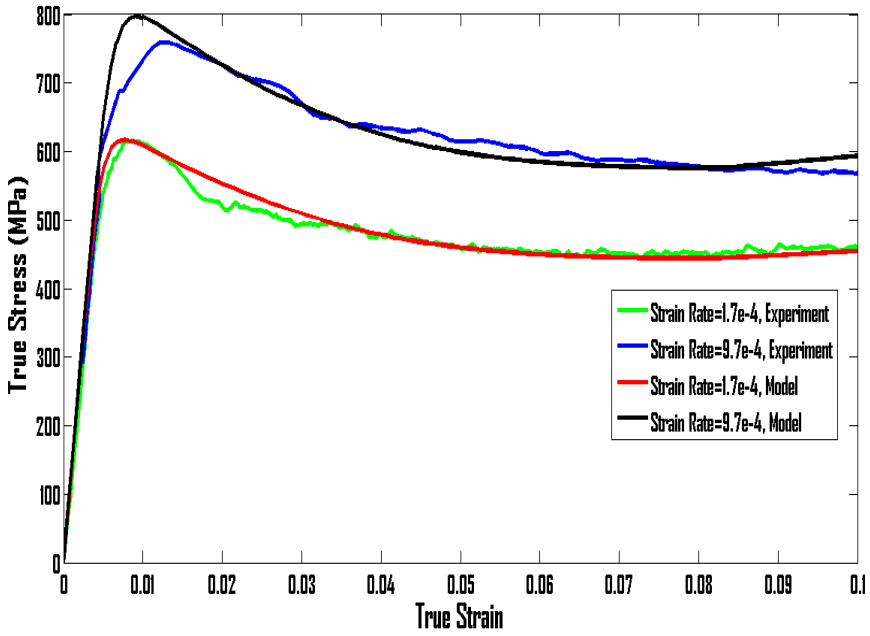
True Stress (MPa)
True Strain
Strain Rate=1.7e-4, Experiment
Strain Rate=9.7e-4, Experiment
Strain Rate=1.7e-4, Model
Strain Rate=9.7e-4, Model

(a)

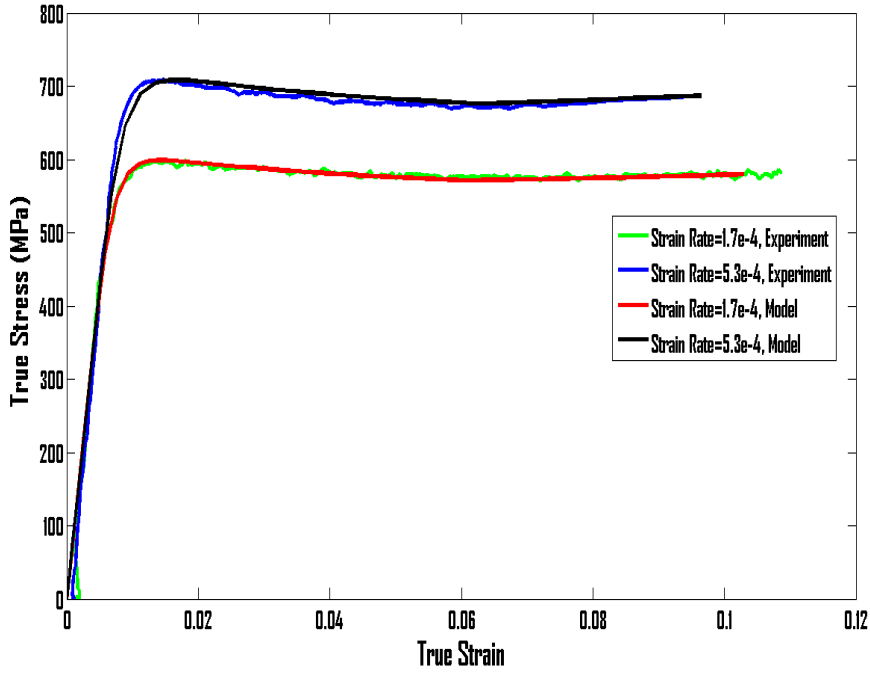
True Stress (MPa)
True Strain
Strain Rate=1.7e-4, Experiment
Strain Rate=5.3e-4, Experiment
Strain Rate=1.7e-4, Model
Strain Rate=5.3e-4, Model

(b)

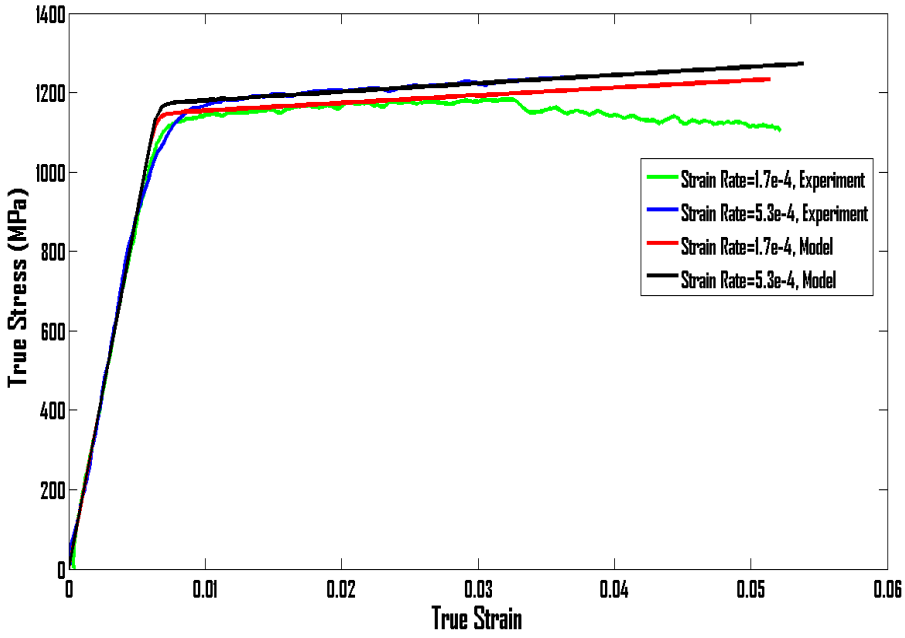

(c)

Fig 3.2 Experimental and calibrated curved for (a) basal <a>, (b) prismatic <a> and (c) pyramidal <c+a>slip systems under different strain rate.

However, due to the different rate sensitivity of single and polycrystalline crystal experiment data, the single calibration results could not be used directly for polycrystalline materials. They could be used as a start point in the polycrystalline calibration.

Chapter 4

3D Polycrystalline microstructural simulation and mesh generation

This chapter discusses the 2D characterization and generation of 3D microstructure models from the 2D data. It has been shown that 3D microstructures can be collected by a number of techniques, such as Focused Ion Beam (FIB) sectioning [15], manual polishing [28] and x-ray methods [29]. But all these methods are somehow tedious and time consuming. The

work here will be based on extrapolation 2D measurements to estimate 3D statistics. This area is known as stereology, which has been under investigation for years [30], and will serve more recent direct 3D techniques to inform the process used in this work.

4.1 Microstructural Characterization of the α Ti-7Al

Three EBSD scans of α Ti-7Al material taken by Air Force Research Lab from 4 orthogonal surfaces were used to characterize the microstructure. Fig 4.1 shows the three EBSD scans.

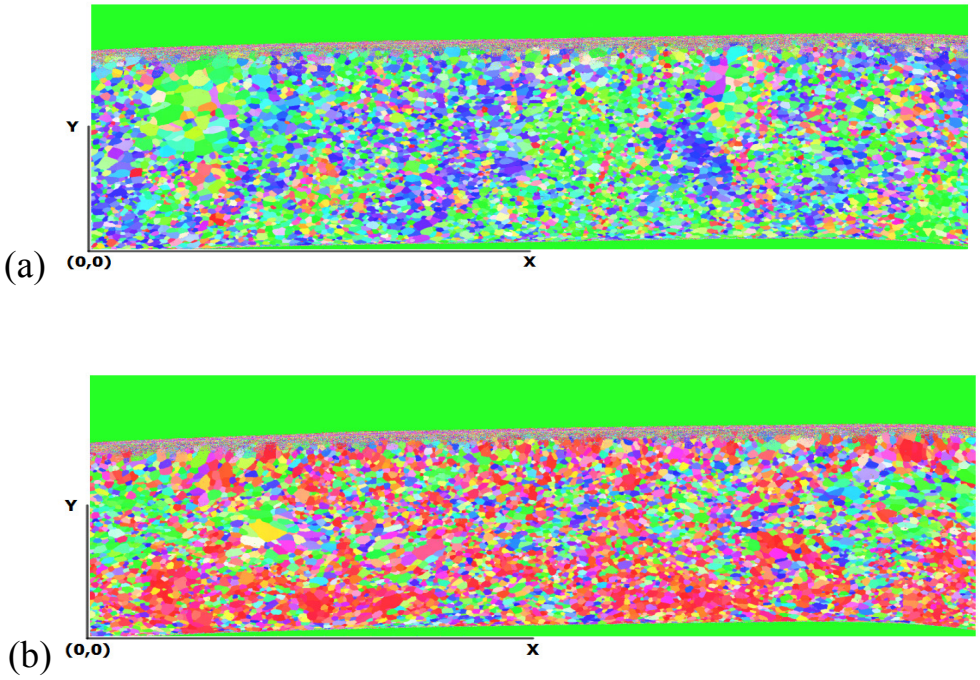

(a)

(b)

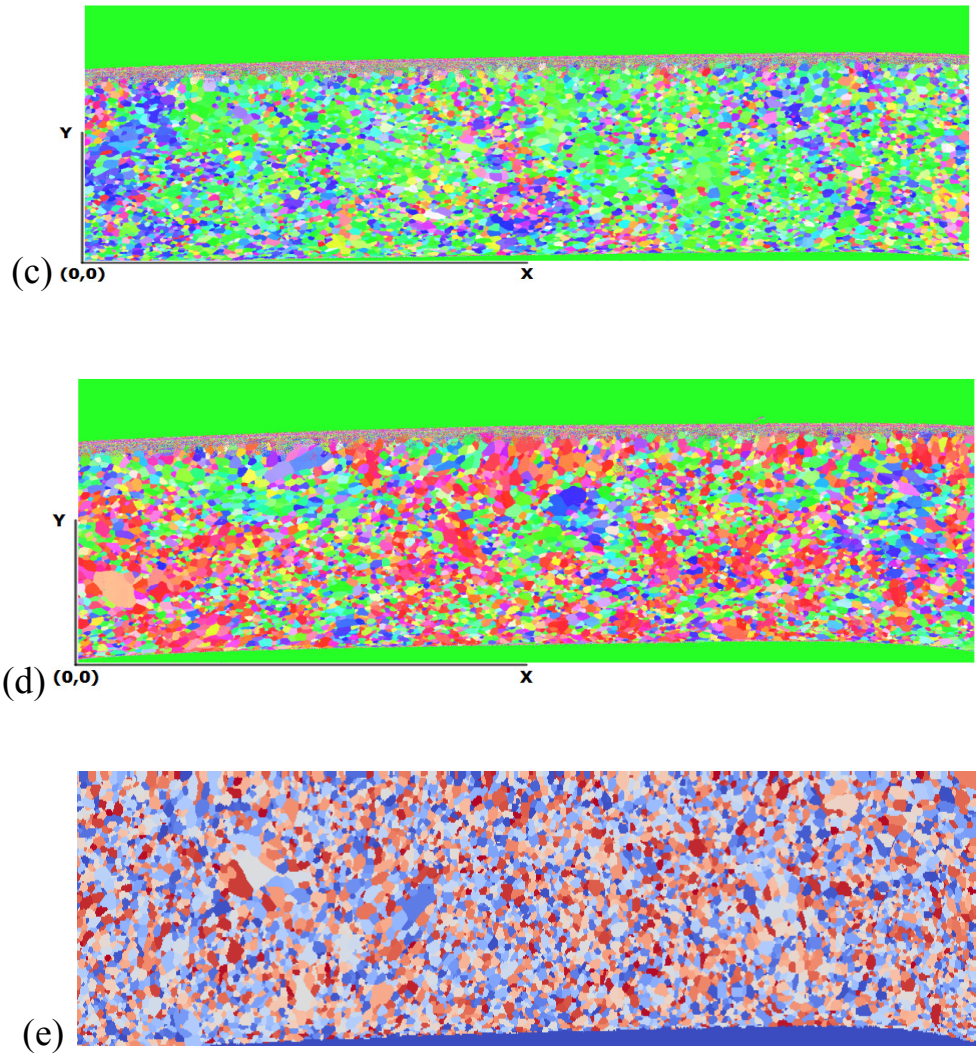

Fig 4.1 EBSD scans of 4 orthogonal surfaces (a) (b) (c) (d) and surface after crop the edge (e)

Using the code described in [14], the EBSD scans from the three orthogonal faces were analyzed to determine a number of crystallographic and morphological microstructural characteristics including size distribution, aspect ratio distribution and principal axis orientation distribution (ellipsoidal-shape grains are assumed), grain size versus number of neighbor

distribution, crystallographic orientation distribution, misorientation distribution and microtexture distribution.

4.2 Microsturctural Simulation Procedures

In order to generate a representative synthetic microstructure that is statistically equivalent to the real microstructure, the microstructural simulation is performed using the code describe in [14].

Grain size is defined by the equivalent sphere diameter (*ESD*). *ESD* is determined by first calculating equivalent circle diameters (*ECD*) using image analysis techniques along with the assumption that the grains are spherical in 3D space and therefore their size can be approximated by the following stereological formula which connects the $\overline{ECD}$ of a sample with the $\overline{ESD}$ of a sample:

$$\overline{ESD} = \frac{4}{\pi}\overline{ECD}$$

According to [15], the lognormal standard probability density function provides a reasonable fit to the grain size data. This function is defined by two parameters, average and standard deviation. For these reasons, the

lognormal standard distribution will be used in this work (see Fig. 4.2) and will be sampled in the synthetic microstructure generation technique to produce statistically equivalent synthetic structures.

In addition to the morphological analysis, the sample of Ti-7Al was analyzed crystallographically. Crystallographic orientation data was obtained through an EBSD scan containing about 10000 grains. Fig. 4.2 provides distribution of size with the number fraction of grains. Fig 4.3 provides the number of neighbors as a function of grain diameter. Fig 4.4 provides HCP orientation with MTEX. as well as misorientation and microtexture distribution. Misorientation is defined from the 2D EBSD scan along the grain boundary length but assumed as equivalent to a grain boundary surface area in the 3D synthetic structure generation. This assumption is reasonable in that matching is done based on a unitless fracture obtained by normalizing the data by either total grain boundary length (in 2D) or total grain boundary surface area (in 3D).

Misorientaton serves as a quantifiable measure of two neighboring voxels orientation difference. The value of misorientation is given by the following equation:

$$\theta = \min \left| \cos^{-1}\left(\frac{tr(g_A g_B O)-1}{2}\right) \right|$$

where $g_A$and $g_B$are the rotation matrics of voxel A and B and are given by:

$$g_i = \begin{pmatrix} cos\varphi_1 cos\varphi_2 - \sin\varphi_1 sin\varphi_2 cos\Phi & sin\varphi_1 cos\varphi_2 + \cos\varphi_1 sin\varphi_2 cos\Phi & sin\varphi_2 sin\Phi \\ -cos\varphi_1 sin\varphi_2 - \sin\varphi_1 cos\varphi_2 cos\Phi & -sin\varphi_1 sin\varphi_2 + \cos\varphi_1 cos\varphi_2 cos\Phi & cos\varphi_2 sin\Phi \\ sin\varphi_1 sin\Phi & -cos\varphi_2 sin\Phi & cos\Phi \end{pmatrix}$$

where $(\varphi_1, \Phi, \varphi_2)$ are the Euler angles of the voxel. O is the symmetry operator, which is a set of 3×3 matrices that account for the symmetry of the crystal. There are 24 matrices for the cubic system of the IN100 material used

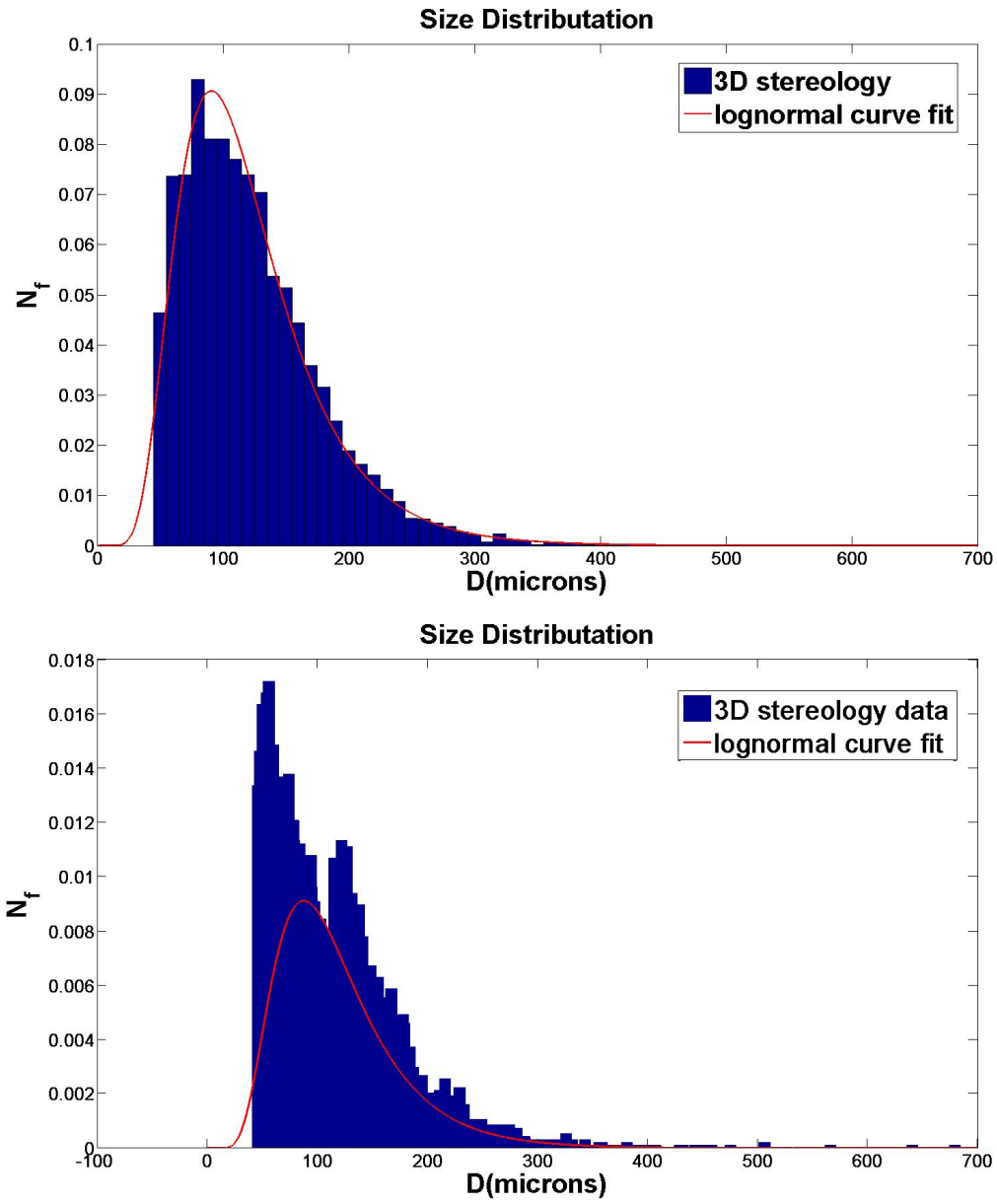

Fig. 4.2 Grain size, D, distribution comparison. N_f is the number fraction of grains/colonies.

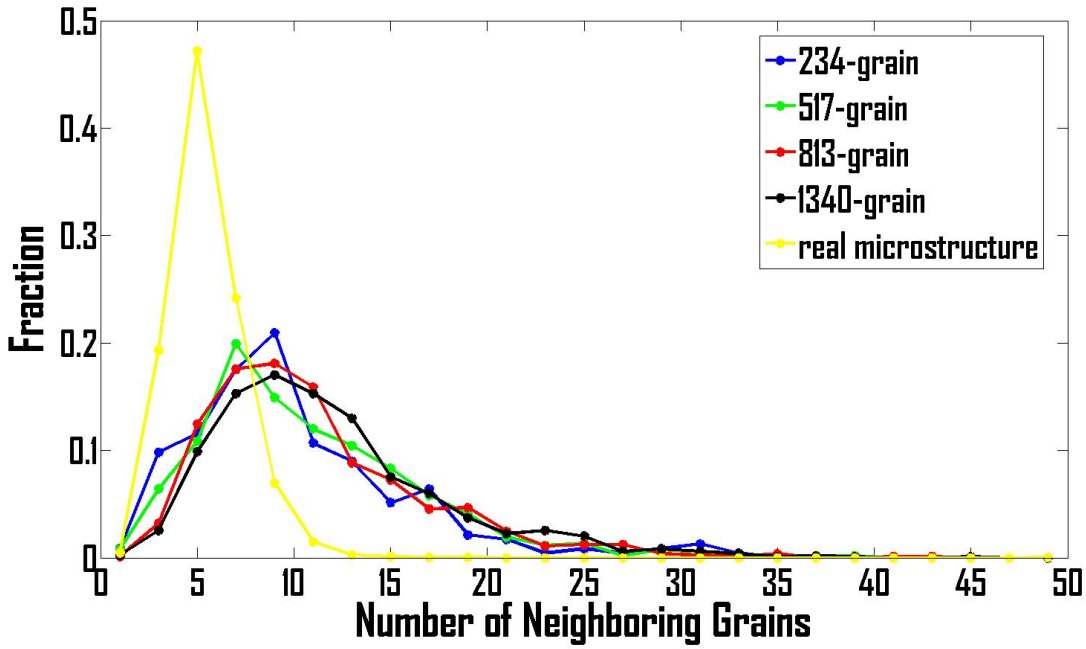

Fig. 4.3 Distribution of number of contiguous neighbors.

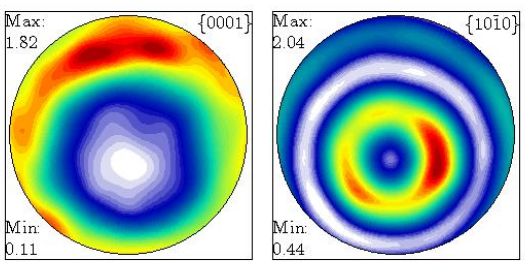

(a)

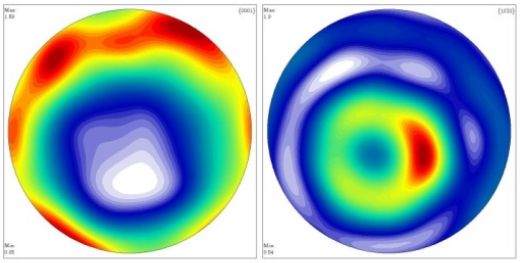

(b)

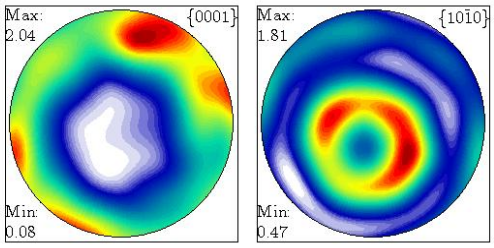

(c)

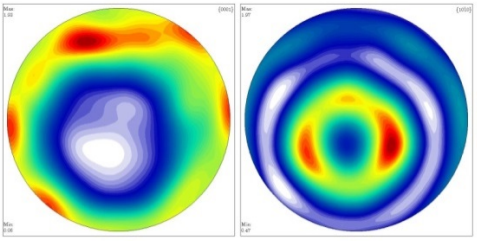

(d)

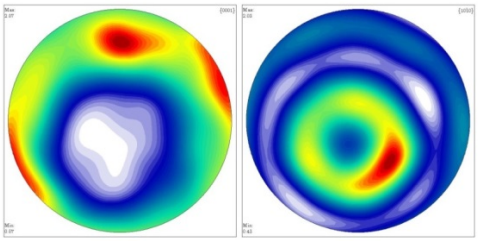

(e)

Fig. 4.4 α phase (0001) and (10$\bar{1}$0) pole figure for (a) Sample data and (b) Synthetic structure with 200 gains (c) Synthetic structure with 500 gains (d) Synthetic structure with 800 gains (e) Synthetic structure with 1000 gains

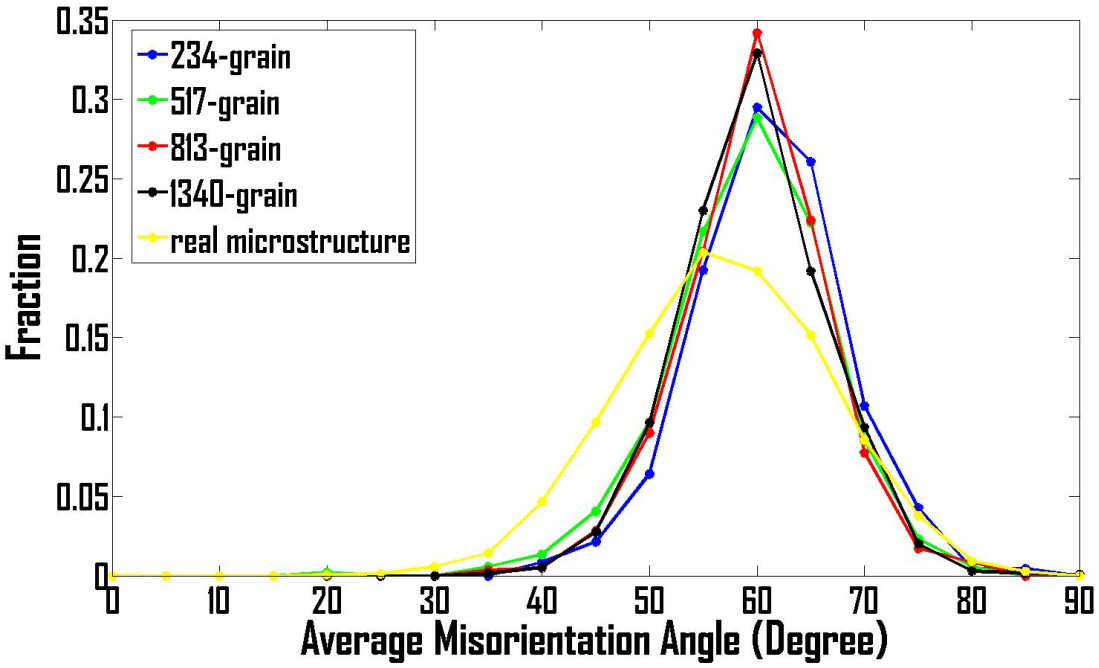

Fig 4.5 Misorientation distribution (MoDF) comparison. Fracture corresponds to either grain boundary length fraction or grain boundary surface area fraction

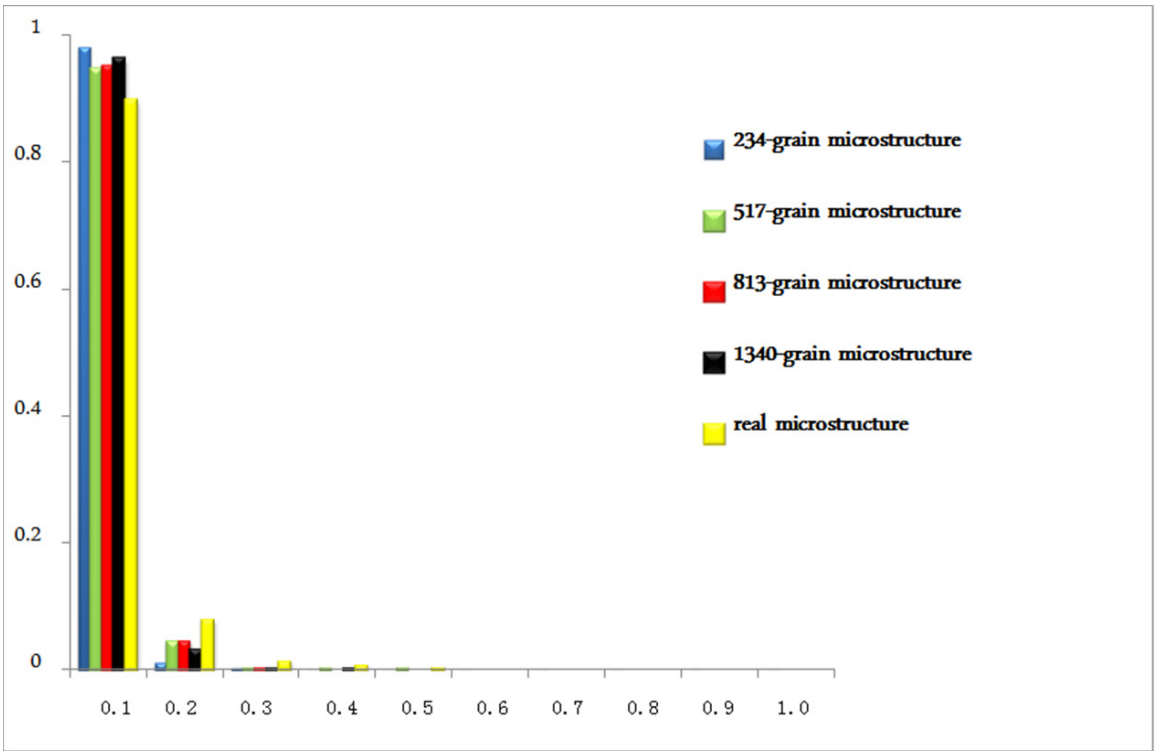

Fig 4.6 Microtexture distribution comparison where microtexture is defined by the number fraction of neighbors with misorientation less than 15°.

The microstructural simulation is performed using the code described in [14] where statistically equivalent microstructures are generated whose morphological and crystallographic statistics are matched. The morphological orientation of the elongated grains was assumed to be random. Grains are placed in the synthetic structure based on neighborhood constraints assuming an average number of neighbors to be approximately 14 grains with a variation according to grain size. This choice was based on

the analysis of IN100 in [16] in 3D, where it was seen that the number of neighbors of a grain correlated strongly to its size. This assumption of correlation between the number of neighbors of a grain to its size implies a lack of clustering of similarly sized grains, which appears to be valid when viewing the 2D micrographs. After the morphological voxelized structure has been built, the grains are assigned HCP orientations based on a random sampling from the ODF. Misorientation and microtexturing statistics are matched by an iterative process. Orientations are allowed to switch between grains or be replaced by new orientation all the while the error is tracked and compared to sample statistics until convergence is attained.

DREAM 3D is used to do the 3D microstructure reconstruction from 2D ang file tested by Dr. Adam Pilchak from Air Force Research Lab. In the first step, ang file is imported into .h5ebsd file which give 2D images (Fig 4.1). In the second step, bad data of the grain is filled out by finding cell quaternions and setting misorientation tolerance and minimum allowed defect size. In the third step, statistics law is added into distribution fitting. For size and neighborhood distribution, log normal fit is inserted and for aspect ratio and omega 3 distribution, beta fit is inserted. Then from the results of step 2, the characteristics of 2D EBSD data such as size, number of neighbors and Euler angle for each grain could be offered. In this way, we

could get the statistic law for size, neighbors, orientation, misorientation, microtexture (Fig 4.2, 4.3, 4.4, 4.5, 4.6). In step 4, synthetic process is undertaken from statistics law from step 3 by finding field phases, surface fields, field neighbors and matching crystallography.

4.3 Microstructural Simulation Validation

The microstructural simulation procedure is validated through comparing the sample statistics with the statistics of the simulated microstructure. Fig. 4.2, 4.3, 4.4, 4.5, 4.6 show statistics of a 200 grain, 500 grain, 800 grain, 1000 grain structure. It has been seen that by 200 grains these statistics have converged to a small error. Structure of 200 grains and above show only slight improvement and because large structures become computationally very expensive, structures of between 200 grains were chosen for the current work.

4.4 Mesh Generation

The resultant 3D microstructure model is a voxelized volume with individual grains having a phase identification and an orientation defined by

3 Euler angles (Fig. 4.7). This voxelized volume needs to be meshed for finite element analysis. 4-noded TET4 element is used here. As this element uses linear interpolation functions, the strains are constant throughout the element and the element is integrated numerically using one point at the centroid of the element. The commercial meshing software, Simmetrix [31], is used to generate the finite element (Fig. 4.7). First a triangular surface mesh is generated along the interior grain boundaries and cube boundaries. Then, this triangular surface element mesh is extended into the full 3D volumetric tetrahedral mesh. The meshes contain 168,403 elements and 30,872 nodes.

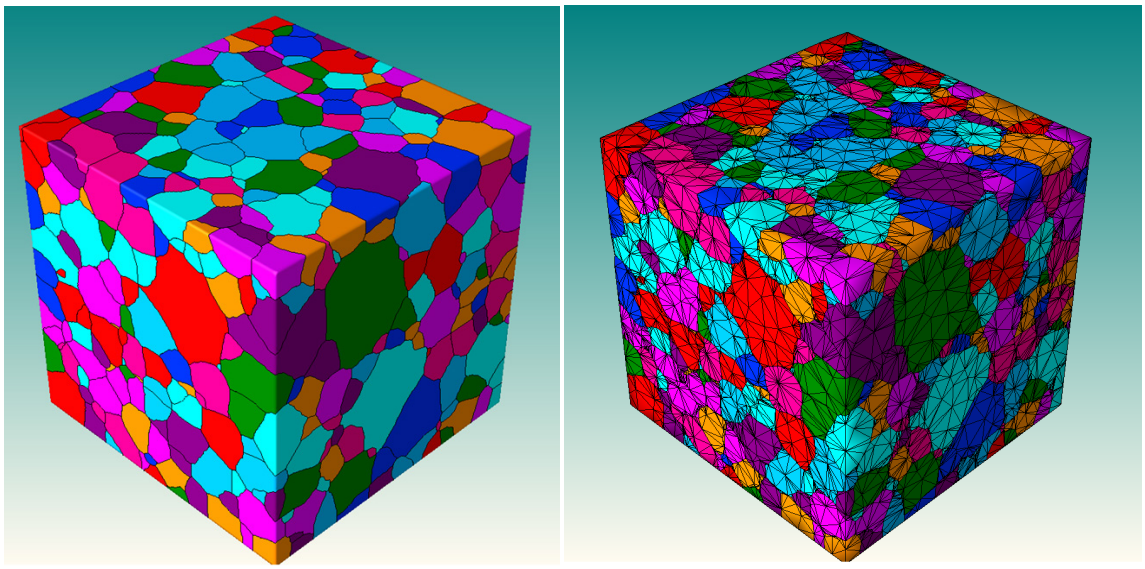

Fig. 4.7 Voxelized volumes before and after meshing for the 1000 grain microstructure. The cube length dimension, l_0, is 1250 μm.

The meshes are checked for distorted elements, which have a very small number of elements with aspect ratio of 80. However because of the expense for computation and the convergence analysis above, 200 grain microstructure (Fig. 4.8) is used in current work for polycrystalline calibration.

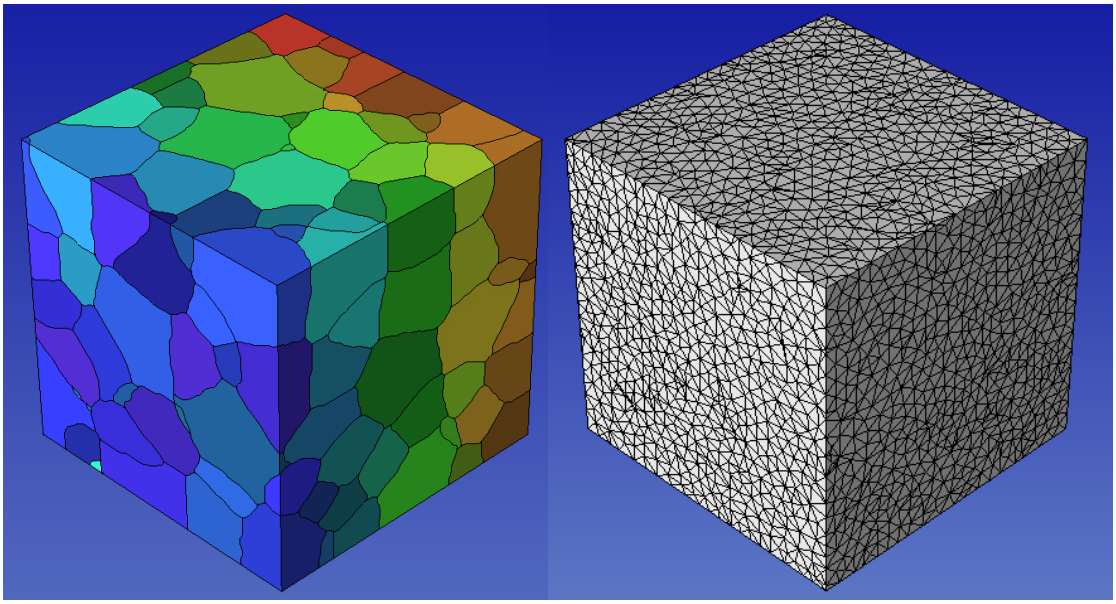

Fig. 4.8 Voxelized volumes before and after meshing for the 200 grain microstructure. The cube length dimension, l_0, is 600 μm.

Chapter 5

Simulation of deformation in polycrystalline Ti-7Al

Constant strain rate test is with strain rate of $4.8\times10^{-4}s^{-1}$ by Dr. Adam Pilchak from Air Force Research Lab. The overall hardening in the polycrystalline Ti-7Al alloy is found to be low. This is attributed to the planar slip due to the presence of short range ordering of Ti and Al atoms, which reduces the rate of hardening as well as the interaction between the different slip systems.

An isothermal, size-dependent and rate-dependent crystal plasticity finite element computational model described and developed in [12, 32, 33] is used with a parallelized code to simulate the response of synthetically generated microstructures of the α-Ti-7Al under constrain strain rate boundary condition.

For simulation of the constant strain rate tests, the engineering strain rate boundary condition is applied. Consistent with the constant engineering strain rate $\dot{\varepsilon}_c$, a displacement boundary condition is applied on the right surface of the cube as

$u(t)=l_0(\dot{\varepsilon}_c t)$

where l_0 is the initial dimension (=600 μm) of the cube. The average stress-plastic strain response in the direction of the applied displacement (X_2) is plotted in Fig. 5.1. The average stress ($\bar{\sigma}_{22}$) and average plastic strain ($\bar{\varepsilon}^p_{22}$) are calculated as

$$\bar{\sigma} = \frac{\sum_{i=1}^{nel}\sum_{j=1}^{npt}(\sigma_{22}J)_{ij}}{\sum_{i=1}^{nel}\sum_{j=1}^{npt}(J)_{ij}}, \bar{\varepsilon} = \frac{\sum_{i=1}^{nel}\sum_{j=1}^{npt}(\sigma_{22}J)_{ij}}{\sum_{i=1}^{nel}\sum_{j=1}^{npt}(J)_{ij}}$$

where σ_{22} and ε^p_{22} are the Cauchy stress and the true strain at each element integration point and *J* is the determinant of the Jacobian matrix at these integration points. The number of elements in the model is designed as *nel*, and *npt* corresponds to the number of integration points per element.

Single crystal calibration result in Chapter 3 is used as the starting point for polycrystalline calibration. The plot in Fig. 5.1 compares the experimental and the computational result for the constant engineering strain rate $4.8\times10^{-4}s^{-1}$. And calibrated parameters for polycrystalline model is shown in Table 5.1

Table 5.1 Calibrated parameters for polycrystalline model

Parameters	Basal <a> slip system	Prismatic <a> slip system	Pyramidal <a> slip system	Pyramidal <c+a>slip system
m	0.15	0.15	0.15	0.02
g_0(MPa)	220	220	330	560
$\dot{\tilde{\gamma}}(s^{-1})$	0.005	0.002	0.002	0.006
h_0	500	300	500	600
r	0.5	0.5	0.5	0.1
n	0.1	0.1	0.1	0.01
$\tilde{g}$(MPa)	500	600	750	1650

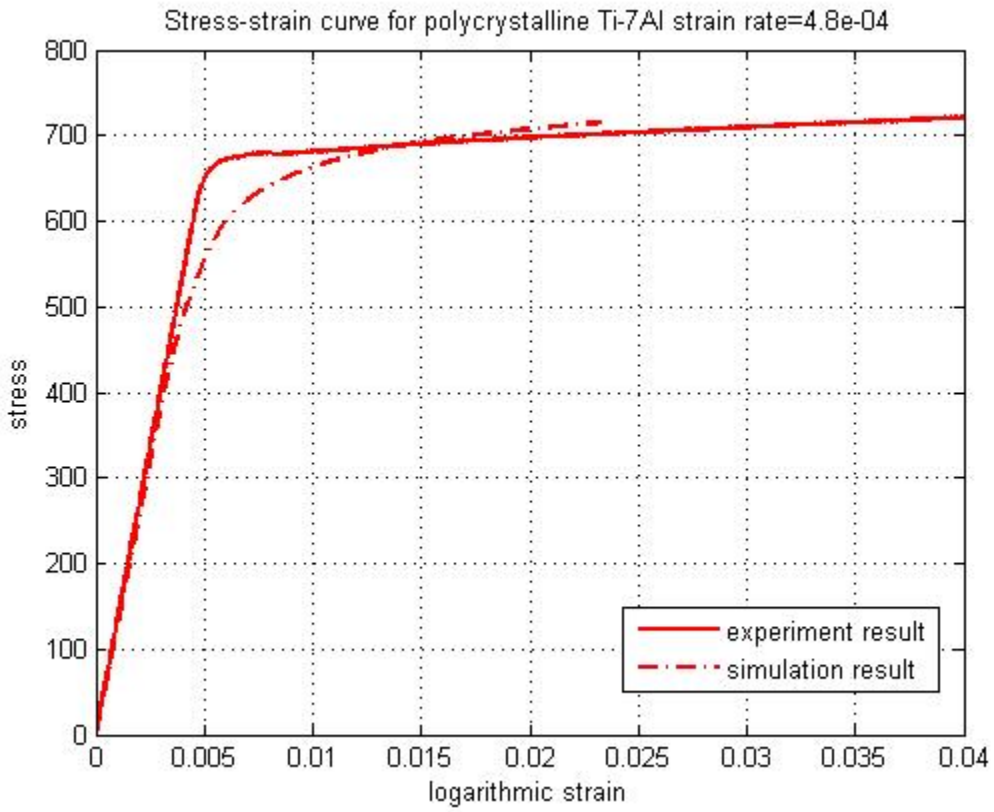

Fig 5.1 Experimental and simulation stress-strain curve with Ti-7Al polycrystalline model under constant strain rate $4.8\times10^{-4}s^{-1}$

Fig. 5.1 shows the comparison for the tensile constant strain rate test. The yield stress is about 680 Mpa. The finite element model is able to capture the behavior of polycrystalline Ti-7Al well. Considering variabilities in the model and the range of time over which the experiments are conducted, the agreement between the experimental and simulated results is good.

Chapter 6

Conclusion

This project is aimed at a systematic development of an experimentally validated crystal plasticity based computationally model of α-Ti-7Al. A rate-dependent crystal plasticity model is incorporated in this model to accommodate anisotropy in material behavior. Ti-7Al only consists of one α phase. A set of behavior including micro testing, computational simulations, and minimization process is implemented in this study for characterization and calibration of material parameters. Elastic and crystal plasticity parameters for crystal slip systems are determined by this process. Then the polycrystalline computational model for Ti-7Al is constructed to incorporate accurate phase volume fractions, and orientation distributions that are statistically equivalent to those observed in OIM scans. The effects of accurate orientation, misorientations and microtexture distributions are investigated through simulations using this computational model. The polycrystalline finite element model is calibrated by comparing the results of simulations with experimental data on constant strain rate.

The capability of this model in capturing microstructural stress-strain evolution is good. In the future work, two particular effects-local orientation

distributions and load shedding, will be investigated. The stress in the loading direction and that normal to the basal plane are important variables governing dwell fatigue crack initiation that are examined. Tests with different constant strain rates and loading direction will be simulated to validate the model. And creep test will also be simulated and compared with experiments. This thesis provides a good understanding of Ti-7Al from a local viewpoint and provides the potential for its being used for developing fatigue failure criteria.

Bibliography

[1] Froes FH, editor. Non-aerospace applications of titanium. Warrendale (PA): TMS; 1998.

[2] Donachie Jr MJ. Titanium-a technical guide. Metals Park (OH): ASM International, 1998.

[3] Adenstedt HK. Metal. Progress 1949; 65: 658.

[4] Inman MA, Gilmore CM. Metall. Trans. 1979; 10:419.

[5] Chu HP. J. Mater. 1970; 5:633.

[6] Odegard BC, Thompson AW. Metall. Trans. 1974; 5:1207.

[7] Miller WH, Chen RT, Starke EA. Metall. Trans. 1987; 18A:1451.

[8] Neeraj T, Mills MJ. Mat. Sci Eng. A-Struct. 2001; 319:415.

[9] Neeraj T, Hou DH, Daehn GS, Mills MJ. Acta Mater. 2000; 48: 1225.

[10] Paton NE, Baggerly RG, Williams JC. AFOSR Report SC526.7FR. 1976.

[11] Balasubramanian S. Polycrystalline plasticity: application to deformation processing of lightweight metals. PhD. dissertation. Cambridge (MA): MIT; 1998.

[12] Hasija V, Ghosh S, Mills MJ, Joseph DS. Acta Mater 2003;51:4533.

[13] Hall EO. Proc Phys Soc London 1951;64:747.

[14] M. Grober. *Development of an automated characterization-representation framework for the modeling of polycrystalline materials in 3D*. PhD thesis, The Ohio State University, 201 West 19th Avenue, Columbus, OH 43210, 2007.

[15] M. Groeber, B.K. Haley, M.D. Uchic, D.M. Dimiduk, and S. Ghosh. Materials Characterization, 57:259-273, 2006.

[16] M. Groeber, S. Ghosh, M. Uchic, and D. Dimiduk. Acta Materialia, 56:1257-1273, 2008.

[17] Peirce D, Asaro RJ, Needleman A. Acta Metall. Mater. 1983; 31:1951.

[18] Asaro RJ, Needleman A. Scripta Metall. Mater. 1984; 18:429.

[19] Harren SV, Asaro RJ. J. Mech. Phys. Solids 1989; 37: 191.

[20] Kalidindi SR, Bronkhorst CA, Anand L. J. Mech. Phys. Solids 1992; 40:537.

[21] Kothari M, Anand L. J. Mech. Phys. Solids 1998; 46:51.

[22] Balasubramanian S, Anand L. Acta Mater. 2002; 50:133.

[23] Goh CH, Wallace JM, Neu RW, McDowell DL. Int. J. Fatigue 2001; 23:S423.

[24] Kad BK, Dao M, Asaro RJ. Mat. Sci. Eng. A-struct. 1995; 193:97.

[25] Petch NJ. J Iron Steel Inst 1953;174:25.

[26] C.L. Xie, S. Ghosh, M. Groeber. Journal of Engineering Materials and Technology, 126: 339-352, 2004.

[27] D. L. Carroll. AIAA Journal, 34:338-346, 1996.

[28] D J Rowenhorst and P W Voorhees. Metallurgical and Materials Transactions A, 36 (August): 2127-2135, 2005.

[29] E Lauridsen, S Schimidt, S Nielsen, L Margulies, H Poulsen, and D Jensen. Scripta Materialia, 55(1): 51-56, 2006.

[30] J. C. Russ and R. T. Dehoff. Practical Stereology. Plenum Press, 2nd edition, 1999.

[31] Simmetrix Inc., Clifton Park, NY 12065. *MeshSim User's Guide*, 2003.

[32] Dhyanjyoti Deka, Deepu S. Josepu, Somnath Ghosh, and Michael J. Mills. *Metallurgical and Materials Transactions* A, 37(5): 1371-1388, 2006.

[33] G. Venkataramani, K. Kirane, and S. Ghosh. International Journal of Plasticity, 24:428-454, 2008.

Curriculum Vitae

Chengcheng Tao received the B. Eng. degree in Civil Engineering from Shanghai Normal University in 2011 and M.S. degree in Civil Engineering from Carnegie Mellon University in 2012.

Chengcheng's research interests lie in the characterization of metal materials. She has worked on project on the mechanism and constitutive models in HCP structure with crystal plasticity analysis with finite element method.